ACS Photonics

pubs.acs.org/journal/apchd5

Article

Enhanced Second-Harmonic Generation in a Monolayer Tungsten Diselenide Integrated Silicon Nitride Nanocavity

Hannah Rarick, Abhinav Kala, Sinabu Pumulo, Arnab Manna, David Sharp, Christopher Munley, Xiaodong Xu, and Arka Majumdar*

Cite This: *ACS Photonics* 2024, 11, 4635–4641

Read Online

ACCESS | Metrics & More | Article Recommendations | Supporting Information

ABSTRACT: Observations of nonlinear optical phenomena are greatly hindered by the large optical power requirements. Nanophotonic cavities can drastically reduce the required optical powers thanks to the strong spatial and temporal confinement of light. Furthermore, two-dimensional atomically thin transition metal dichalcogenides boast high nonlinear optical coefficients and are promising candidates for hybrid nanophotonics due to their ease of integration and compatibility with many substrates without requiring explicit lattice matching. Here, we demonstrate cavity enhanced second harmonic generation in a monolayer tungsten diselenide integrated silicon nitride nanocavity. With a fundamental frequency close to the excitonic resonance and a large second order susceptibility at wavelengths near 800 nm, we observed a cavity enhancement of more than 3 orders of magnitude of second harmonic generation compared to bare monolayer.

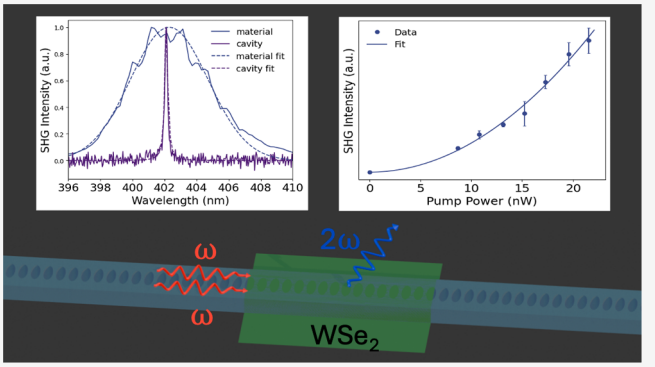

KEYWORDS: *2D materials, nonlinear optics, photonic nanocavity*

INTRODUCTION

Nonlinear optical (NLO) effects are pivotal in the advancement of optical information processing.[1,2] Previous works have shown that nonlinear phenomena like second-harmonic generation (SHG) and spontaneous parametric down conversion (SPDC) are relevant for light converters and light sources with applications in sensing, all-optical communication, and quantum information science and technology.[2−7] Such NLO processes can be attributed to higher order terms in the power series expansion of the polarization field, $P(t) = \epsilon_0(\chi^{(1)}E(t) + \chi^{(2)}E^2(t) + \chi^{(3)}E^3(t) + ...)$ where ϵ_0 is the permittivity of free space, $\chi^{(n)}$ is the n^{th} order susceptibility, and $E(t)$ is the electric field. SHG, also known as frequency doubling, is a second order nonlinear process in which two photons of the same energy ($\hbar\omega_1$) interact with a nonlinear material to create an output photon with the energy $\hbar\omega_2$, such that $\hbar\omega_2 = 2\hbar\omega_1$. For these processes, required nonzero $\chi^{(2)}$ susceptibility exists only for noncentrosymmetric crystalline structures.[8,9] Observation of SHG is critical for quantum and classical information science, including observation of optical bistability, quantum frequency conversion and frequency combs.[10−12] The primary obstacle to observing these NLO phenomena stems from the weak nonlinear susceptibilities of bulk materials, which demand large optical power. The emergence of low-dimensional materials like quantum dots and two-dimensional (2D) materials have introduced alternative routes to achieving NLO effects with relaxed phase-matching conditions.[3−5,7,8,13−25] Especially, integrating these low-dimensional materials onto photonic platforms can enable on-chip NLO effects with drastically reduced power requirements compared with traditional bulk material systems. Such low-power NLO systems will have promising applications in miniaturizing information processing, sensing, and quantum information technologies. Transition metal dichalcogenide (TMD) monolayers are atomically thin 2D with composition MX_2, where M is a transition metal and X is a chalcogen. Single or few-layer TMDs are ideal for heterogeneous integrated photonics due to their ease of integration, mechanical robustness, large exciton binding energies, and bandgap variability.[3,7,8,26−29] The broken inversion crystal symmetry of a variety of monolayer TMDs offer high $\chi^{(2)}$ susceptibilities, particularly near their excitonic resonances.[8,13,18,23,26] Furthermore, monolayer tungsten diselenide (WSe_2) proves to be an ideal candidate for SHG due to its large $\chi^{(2)}$ value at 800 nm ($d_{eff} \approx 5$ nmV^{-1}).[13]

Researchers have utilized the large susceptibilities of monolayer TMDs using various platforms such as plasmonic

Received: June 4, 2024
Revised: October 23, 2024
Accepted: October 24, 2024
Published: November 2, 2024

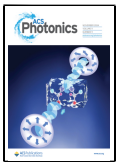

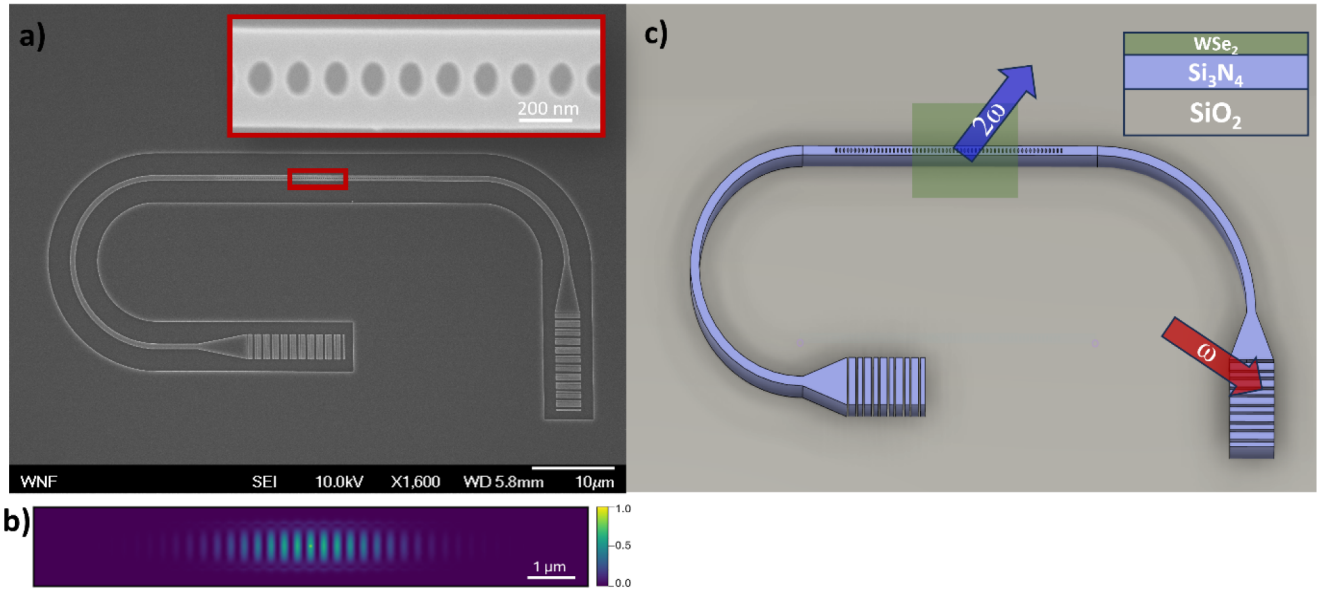

Figure 1. Overview of experiment. (a) Scanning electron micrograph image of a nanobeam where the inset is the magnified view of the highlighted region in red. (b) Electric field profile of the fundamental cavity mode simulated using finite difference time domain (FDTD) simulation methods. (c) Illustration of experiment where laser is coupled through the grating (red) into the cavity and SHG is collected from the top of the cavity (blue). The highlighted region in green depicts the placement of monolayer WSe_2. The inset in the top right illustrates the material stack in the cavity region.

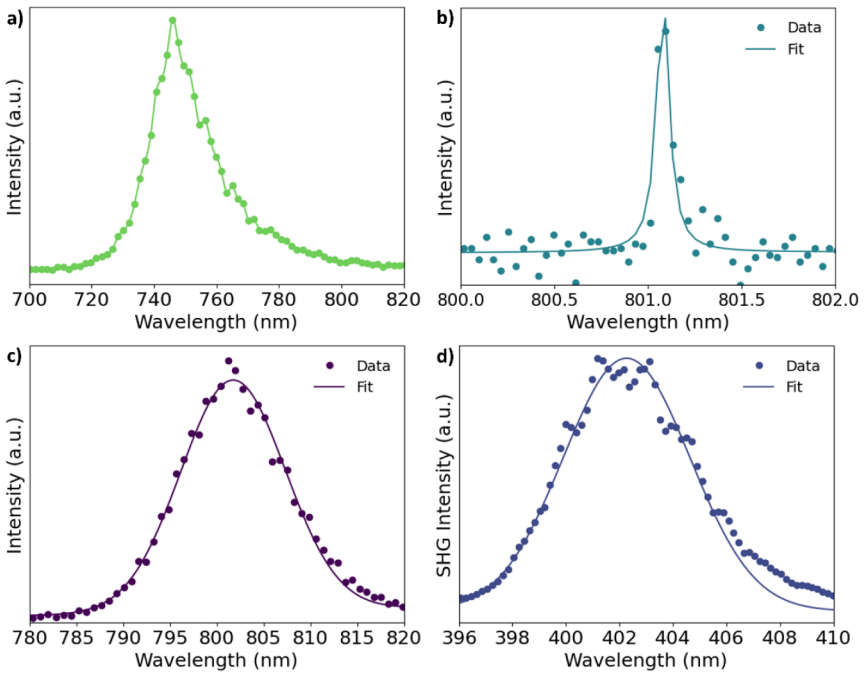

Figure 2. Characterization of the Nanobeam and Monolayer WSe_2. (a) Room temperature photoluminescence measurement of monolayer WSe_2 using a 532 nm continuous wave diode-pumped solid-state laser. (b) Transmission of the nanobeam with the cavity mode at 801 nm and a Q-factor of ~10,000. (c) Ti:sapphire spectra (dotted) and fitting (solid) used for SHG measurements centered at 801.74 nm with a repetition rate of 80 MHz and pulse width of 100 fs. (d) SHG from bare monolayer WSe_2 centered at 402.3 nm.

cavities, microresonators, metasurfaces, nanowires, and photonic crystal defect cavities to demonstrate up to 3 orders of magnitude enhancement in NLO processes.[14,30−40] To maximize the enhancement of the NLO processes, several points should be considered. First, a large electric field intensity is required, which is achievable in a low mode volume cavity. Second, long interaction times between the material and cavity are desired to enhance the overall effective nonlinearity. For this consideration, the cavity requires large quality factors (Q factors).[41] Plasmonic cavities, while possessing small mode volumes, tend to have small quality factors. Due to the lossless nature of dielectric materials, systems like metasurfaces and microresonators offer large Q factors but also have large mode volumes. Dielectric cavities with small mode volumes and high Q factors overcome both of these limitations and can provide a promising way for enhancing optical nonlinear effects.[30,42,43] In

https://doi.org/10.1021/acsphotonics.4c01029
ACS Photonics 2024, 11, 4635−4641

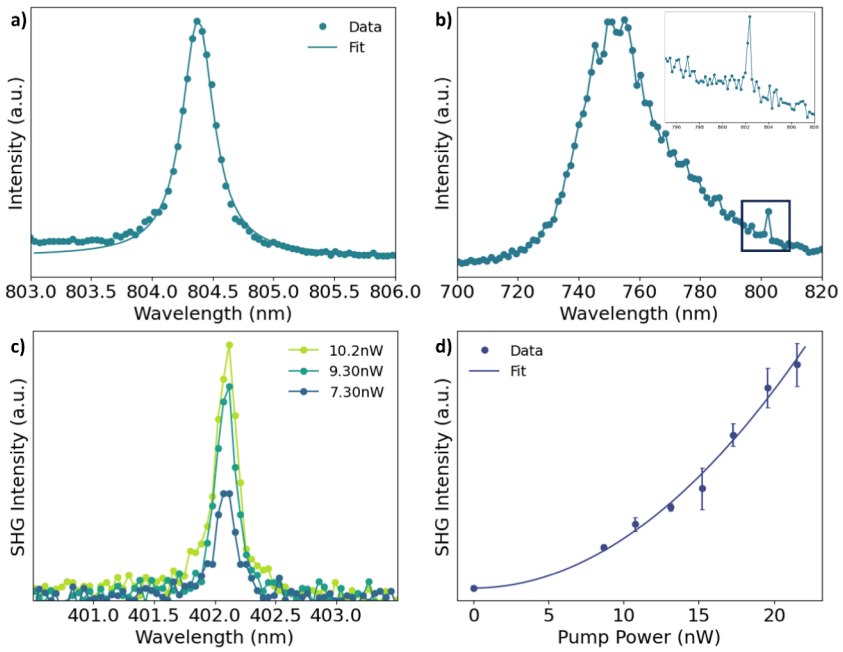

Figure 3. Characterization of Monolayer WSe_2− SiN Nanobeam System. (a) Transmission of the nanobeam cavity after integration of monolayer WSe_2. The cavity mode shifted to ∼804 nm with a Q-factor of ∼2600. (b) Room temperature photoluminescence measurement of a monolayer WSe_2−SiN nanobeam system using a 532 nm continuous wave diode-pumped solid-state laser. The inset shows the boxed region of the spectrum. (c) SHG in monolayer WSe_2−SiN nanobeam system from 7.3 9.3, and 10.2 nW powers. (d) Subsequent quadratic fitting (solid) of SHG power series measurement (dotted).

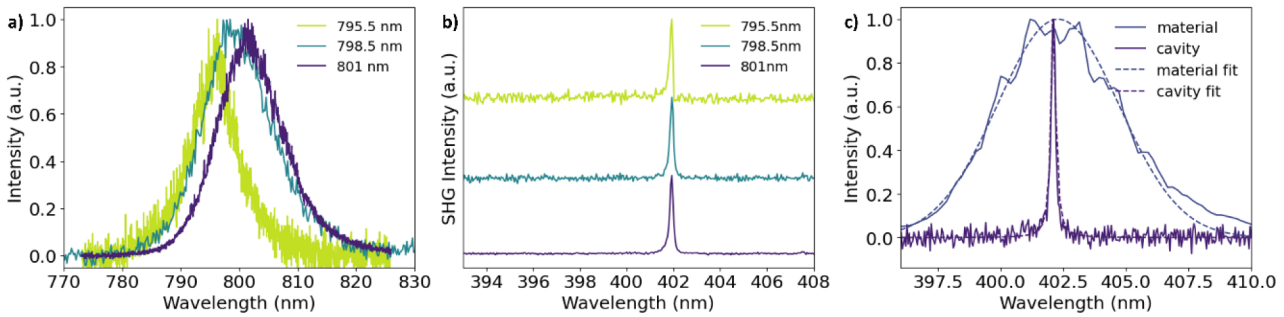

Figure 4. Comparison of SHG. (a) Ti:sapphire with repetition rate of 80 MHz and pulse width of 100 fs spectrum centered at 795.5 nm (green), 798.5 nm (blue), and 801 nm (purple). (b) Subsequent waterfall plot of SHG exhibited from nanobeam-monolayer WSe_2 system using varied Ti:sapphire spectrum centered at 795.5 nm, 798.5 nm, and 801 nm. The SHG for all Ti:sapphire spectra exhibited a peak at $\lambda \sim 402$ nm. (c) Comparison of normalized SHG generated from monolayer WSe_2 (blue) and SiN nanobeam-monolayer WSe_2 system (purple) and their respective fittings (dotted). The fitting of the full width at half-maximum (FWHM) for the monolayer WSe_2 was 5.75 ± 0.15 nm, while the cavity enhanced FWHM was 0.19 ± 0.01 nm.

this paper, we utilize a photonic crystal nanobeam cavity to enhance SHG of a monolayer WSe_2 (Figure 1a,b). Our choice of an on-substrate silicon nitride (Si_3N_4) nanobeam offers mechanical robustness and a wide bandgap which supports transmission in the visible to near-infrared range ideal for integration of monolayer WSe_2. Furthermore, the WSe_2 monolayer integrated silicon nitride platform preserves compatibility with standard silicon-based semiconductor fabrication processes. With the fundamental cavity mode near the excitonic resonance and transparency of silicon nitride at both fundamental and second harmonic wavelengths, the monolayer WSe_2−SiN nanobeam system shows promise in delivering a stronger nonlinear response.

As shown in Figure 1c, SHG measurements of the monolayer WSe_2-nanobeam system were conducted by illuminating a grating coupler using a Ti:sapphire pulsed laser while collecting the SHG signal from the top of the cavity. Prior to the cavity-coupled experiments, the bare cavity and material were characterized independently. To confirm the quality of the monolayer WSe_2 flake, room temperature photoluminescence was collected of the monolayer WSe_2 on 220 nm silicon nitride layer on 4 μm of oxide on silicon, and emission was observed from 720 to 800 nm (Figure 2a). To assess the quality and fundamental mode of the nanobeam cavity, transmission measurements of the bare nanobeam confirmed a cavity mode at ∼801 nm with a Q factor of ∼10,000 (Figure 2b). Figure 2c shows the Ti:sapphire laser's Gaussian spectral profile, used for the SHG measurements, centered at roughly ∼800 nm. The Ti:sapphire pulsed laser operated with a repetition rate of 80 MHz and a pulse width of 100 fs. Lastly, SHG signal of the bare monolayer WSe_2 was confirmed on unpatterned oxide over silicon and exhibited a central peak at ∼402.3 nm (Figure 2d). A control sample of

https://doi.org/10.1021/acsphotonics.4c01029
ACS Photonics 2024, 11, 4635−4641

WSe_2 on bare oxide allowed the same flake to be transferred onto the nanobeam.

RESULTS

After integration of the monolayer WSe_2, transmission and cavity coupled photoluminescence measurements were performed to characterize the monolayer WSe_2−SiN nanobeam system (Figure 3a,b). There was an observed shift in the cavity mode to ∼804 nm with a diminished quality factor of ∼2600 (Figure 3a). Degradation of the quality factor is due to the absorbance of the WSe_2 and the remaining residue of the monolayer WSe_2 transfer process.[30] The cavity enhanced SHG signal exhibited a central peak at ∼402 nm. The power series estimated from the power in the cavity and the subsequent quadratic fitting are shown in Figure 3c,d, respectively. In Figure 3d, the error bars for the quadratic fitting were determined by using the upper and lower fitting estimates. To confirm the cavity enhancement of the SHG signal, we measured the SHG by varying the Ti:sapphire center wavelength. Three different laser wavelengths centered at 795.5 nm, 798.5 nm, and 801 nm and their corresponding SHG signals are illustrated in Figure 4a,b, respectively. Irrespective of the Ti:sapphire pulsed laser peak, the SHG signal was centered at ∼402 nm confirming that enhanced SHG signals only occur at half the cavity wavelength and thus originates from the cavity mode. Figure 4c illustrates the approximate line width narrowing observed from the cavity enhanced SHG from 5.75 nm ±0.15 nm (monolayer WSe_2) to 0.19 nm ±0.01 nm (SiN nanobeam-monolayer WSe_2 system). Further full width at half-maximum (FWHM) analysis can be found in Section S1.

To estimate the SHG efficiency, we first estimate the number of photons at the fundamental frequency that enters the cavity. We model the cavity as a Fabry−Perot cavity with two loss channels−cavity mirror loss and other scattering losses with loss rates κ and γ, respectively. We assume that the laser power after the objective is P. After passing through the objective, the pump laser experiences losses at the gratings, in the waveguide, and in the cavity mirrors. Additionally, it is spectrally filtered via a cavity transmission function. We assume the cavity mode angular frequency is ω_c, the grating coupler efficiency is g, the transmission of the waveguide is t_w, and the fraction of pump energy within the cavity mode spectrum is f. With these parameters, the number of photons incident on the cavity from waveguide per unit time is given by

$$N_p = \frac{P \times g \times t_w \times f}{\hbar\omega_c} \quad (1)$$

Using cavity input-output relations, we estimate the number of photons entering the cavity per unit time, N_c (Section S2). We found that the photon entrance rate was $N_c = 0.037N_p$. To get the value of N_p, we used eq 1 where g and t_w were estimated by FDTD simulations to be 0.055 and 0.99 (at resonance), respectively. To estimate the value of f, we multiplied the cavity mode profile obtained from experiments with the laser spectrum to obtain a product curve. The ratio of area under the product curve to the area under the laser spectrum curve is equal to f which we found to be 0.023. Combining all the parameters together, using eq 1, we get $N_c = P \times 1.9 \times 10^{14}$. Where the unit of P is Watts. We call the power coupled into the cavity, P_{cavity}. An input power of 10 mW corresponds to $N_c = 1.9 \times 10^{12}$ and $P_{cavity} = 465\ nW$

To estimate the generated second harmonic power, we correlated the spectrometer counts with the power collected by the objective by sending a 400 nm CW laser in the collection path. The relation between counts on the spectrometer CCD and the collected power (P_{SHG}) was established. For an incident power of 10 mW, the collected SHG power at the objective was 223 fW. The SHG enhancement factor (EF) was estimated by comparing the SHG efficiency for monolayer WSe_2 on the cavity and on an unpatterned SiN film. If P_{ref} is the pump power for the reference SHG measurement on WSe_2 over unpatterned SiN and P_{SHGref} is the corresponding collected SHG power, $EF = \frac{P_{SHG}}{P_{cavity}^2} \times \frac{P_{ref}^2}{P_{SHGref}}$. For the reference monolayer WSe_2, 65.8 pW of SHG power was collected at the objective by using a pump power of 857 μW. With these reference values, we got $EF = 8.95 \times 10^3$. Since our numerical estimations give us the upper limit on the power coupled to the cavity mode, this enhancement factor is a lower bound of the actual value.

CONCLUSION

We experimentally demonstrated more than 3 orders of magnitude enhancement of SHG efficiency from monolayer WSe_2 by integrating it in a low mode volume silicon nitride nanobeam cavity. A key future direction of this work is to reduce the pump loss and increase the second harmonic collection efficiency. A possible solution is to leverage evanescently coupled waveguides for both pump and the second harmonic collection.[44] This work can contribute toward the advancement of various on-chip nonlinear photonic phenomena essential for information processing, sensing, and communication.

EXPERIMENTAL SECTION

Design of Nanobeam. To determine the ideal width and thickness of a SiN waveguide at 800 nm, we conducted Finite Difference eigenmode (FDE) simulations. We found the optimal width and thickness of the SiN nanobeam to be 600 nm and 220 nm, respectively. Using FDTD simulations, we optimized the design of a silicon nitride nanobeam for fundamental transverse electric (TE) cavity mode with a wavelength of 800 nm. As shown in Figure 1a, the nanobeam cavity consists of a waveguide with periodic elliptical air holes. The outermost holes act as a Bragg mirror that confines the light the cavity. The central region of the cavity is formed by the quadratic tapering of the periodicity of the holes.[42] The major and minor radii of the elliptical air holes are 140 and 50 nm, respectively. The Bragg mirror region consists of 20 periods (a_{Bragg} = 266.32 nm) of air holes. Similarly, the quadratic tapering of periodicity in the central holes occurs over 10 periods with the smallest period being a_{taper}= 245.9 nm. The theoretical quality factor of this design was ∼15,000. To characterize the transmission of the nanobeam, the gratings were designed using FDTD simulations. The simulations optimized the duty cycles and pitches of the gratings for maximal coupling at 800 nm.

Fabrication of Silicon Nitride Nanobeams. Fabrication of our devices and integration of the monolayer WSe_2 follow similar procedures to those described in previous works.[30] A 10 mm × 10 mm 220 nm SiN on a 4 μm oxide chip was prepared by a series of acetone and isopropanol sonication baths. ZEP 520 A was then deposited using a spin coater at

https://doi.org/10.1021/acsphotonics.4c01029
ACS Photonics 2024, 11, 4635−4641

3000 rpm for 60 s and subsequently baked for 3 min at 180 °C. The ZEP 520 A was patterned using a JEOL-JBX6300FS 100 kV electron-beam lithography system. The SiN sample was then developed using amyl acetate and isopropanol. The nanobeam was then etched using a fluorine gas based inductive coupled plasma reactive ion etching (ICP-RIE) process. Finally, the remaining resist was removed by sequentially submerging the sample in dichloromethane, acetone, and isopropyl alcohol.

Integration of Monolayer WSe_2 Onto Nanobeam. A maximum of the SHG signal of the monolayer WSe_2 occurs when the polarization of the incident light is aligned to the arm-chair axis.[13] During the transfer, careful alignment of the flake ensured that the armchair axis was aligned to the polarization of the nanobeam cavity TE mode. By dry transfer using a polydimethylsiloxane (PDMS) stamp, the flake was placed on the central region of the nanobeam cavity. Lastly, the monolayer WSe_2-nanobeam system was submerged in chloroform to dissolve remaining residue and was gently dried with nitrogen. More information about sample preparation and characterization can be found in Section S4.

Characterization of Nanobeam. To account for fabrication imperfections, a wide array of nanobeams with variable cavity mode wavelengths were fabricated to select the ideal nanobeam candidate for monolayer WSe_2 integration. The cavity modes of the nanobeams ranged from 790−820 nm with quality factors from ∼6,000−10,000. After the characterization of the nanobeam array, the nanobeam with a suitable cavity mode wavelength and the highest Q factor was selected as the ideal nanobeam candidate.

Experimental Setup. Measurements of transmission, photoluminescence, and second harmonic generation were conducted using the same optical setup via a scanning mirror, removable filters, polarizers and flip mirrors. A detailed setup schematic can be found in Section S3. Transmission spectra were collected by using a FIANIUM supercontinuum laser by exciting and collecting from the gratings. The use of polarizers in the collection and excitation pathways enabled exploitation of the cross-polarized nature of the nanobeam gratings. Cavity coupled room temperature photoluminescence spectra were collected by using a 532 nm DPSS laser excitation into the central region of the cavity. The collection and excitation regions were concentric. Furthermore, using a scanning mirror enabled us to collect a scanning photoluminescence map of both our monolayer WSe_2 flake and monolayer WSe_2−SiN nanobeam system. Second harmonic generation measurements were conducted using a Spectra Ti:sapphire laser (Tsunami by Spectra Physics) with a repetition rate of 80 MHz and a pulse width of 100 fs. All optical setups utilized a 100× objective with NA = 0.9 from Zeiss.

■ ASSOCIATED CONTENT

Supporting Information

The Supporting Information is available free of charge at https://pubs.acs.org/doi/10.1021/acsphotonics.4c01029.

An investigation into the full width at half-maximum (FWHM) of our cavity system both before and after integration of monolayer WSe_2 is provided in Supporting Information section S1. Furthermore, a detailed derivation and explanation of our cavity photon number estimation and schematic of the cavity model can be found in Supporting Information section S2. A thorough explanation and illustration of the optical setups used for measurements in our experiment can be found in Supporting Information section S3. Lastly, information relating to the material fabrication and characterization is provided in Supporting Information section S4 (PDF)

■ AUTHOR INFORMATION

Corresponding Author

Arka Majumdar − *Department of Physics, University of Washington, Seattle, Washington 98195, United States; Department of Electrical and Computer Engineering, University of Washington, Seattle, Washington 98195, United States;* orcid.org/0000-0003-0917-590X; Email: arka@uw.edu

Authors

Hannah Rarick − *Department of Physics, University of Washington, Seattle, Washington 98195, United States*

Abhinav Kala − *Department of Electrical and Computer Engineering, University of Washington, Seattle, Washington 98195, United States*

Sinabu Pumulo − *Department of Material Science Engineering, University of Washington, Seattle, Washington 98195, United States*

Arnab Manna − *Department of Physics, University of Washington, Seattle, Washington 98195, United States;* orcid.org/0009-0007-0056-9650

David Sharp − *Department of Physics, University of Washington, Seattle, Washington 98195, United States;* orcid.org/0000-0002-1034-8567

Christopher Munley − *Department of Physics, University of Washington, Seattle, Washington 98195, United States;* orcid.org/0000-0001-5684-3144

Xiaodong Xu − *Department of Physics, University of Washington, Seattle, Washington 98195, United States; Department of Material Science Engineering, University of Washington, Seattle, Washington 98195, United States;* orcid.org/0000-0003-0348-2095

Complete contact information is available at: https://pubs.acs.org/10.1021/acsphotonics.4c01029

Funding

Funding for this research is supported by National Science Foundation grants NSF-1845009, NSF-2103673, and NSF-ECCS-1708579. Additional funding from the National Science Foundation provided research fellowship support through grant DGE-2140004. Part of this work was conducted at the Washington Nanofabrication Facility/Molecular Analysis Facility, a National Nanotechnology Coordinated Infrastructure (NNCI) site at the University of Washington with partial support from the National Science Foundation via awards NNCI-1542101 and NNCI-2025489.

Notes

The authors declare no competing financial interest.

■ REFERENCES

(1) Leuthold, J.; Koos, C.; Freude, W. Nonlinear Silicon Photonics. *Nat. Photonics* **2010**, *4* (8), 535−544.

(2) Gibbs, H. *Optical Bistability: Controlling Light With Light*; Elsevier Science: Saint Louis, 2014.

(3) Turunen, M.; Brotons-Gisbert, M.; Dai, Y.; Wang, Y.; Scerri, E.; Bonato, C.; Jöns, K. D.; Sun, Z.; Gerardot, B. D. Quantum Photonics with Layered 2D Materials. *Nat. Rev. Phys.* **2022**, *4* (4), 219−236.

(4) Chen, Y.; Sharp, D.; Saxena, A.; Nguyen, H.; Cossairt, B. M.; Majumdar, A. Integrated Quantum Nanophotonics with Solution-Processed Materials. *Adv. Quantum Technol.* **2022**, *5* (1), 2100078.
(5) Seyler, K. L.; Schaibley, J. R.; Gong, P.; Rivera, P.; Jones, A. M.; Wu, S.; Yan, J.; Mandrus, D. G.; Yao, W.; Xu, X. Electrical Control of Second-Harmonic Generation in a WSe2Monolayer Transistor. *Nat. Nanotechnol.* **2015**, *10* (5), 407−411.
(6) McMahon, P. L. The Physics of Optical Computing. *Nat. Rev. Phys.* **2023**, *5* (12), 717−734.
(7) Autere, A.; Jussila, H.; Dai, Y.; Wang, Y.; Lipsanen, H.; Sun, Z. Nonlinear Optics with 2D Layered Materials. *Adv. Mater.* **2018**, *30* (24), 1705963.
(8) Zhang, J.; Zhao, W.; Yu, P.; Yang, G.; Liu, Z. Second Harmonic Generation in 2D Layered Materials. *2D Mater.* **2020**, *7* (4), 042002.
(9) Boyd, R. W. *Nonlinear Optics*, 3rd ed.; Academic Press: Amsterdam, Boston, 2008.
(10) Fryett, T. K.; Dodson, C. M.; Majumdar, A. Cavity Enhanced Nonlinear Optics for Few Photon Optical Bistability. *Opt. Express* **2015**, *23* (12), 16246.
(11) Lu, J.; Li, M.; Zou, C.-L.; Al Sayem, A.; Tang, H. X. Toward 1% Single-Photon Anharmonicity with Periodically Poled Lithium Niobate Microring Resonators. *Optica* **2020**, *7* (12), 1654.
(12) Szabados, J.; Puzyrev, D. N.; Minet, Y.; Reis, L.; Buse, K.; Villois, A.; Skryabin, D. V.; Breunig, I. Frequency Comb Generation via Cascaded Second-Order Nonlinearities in Microresonators. *Phys. Rev. Lett.* **2020**, *124* (20), 203902.
(13) Ribeiro-Soares, J.; Janisch, C.; Liu, Z.; Elías, A. L.; Dresselhaus, M. S.; Terrones, M.; Cançado, L. G.; Jorio, A. Second Harmonic Generation in WSe $_2$. *2D Mater.* **2015**, *2* (4), 045015.
(14) Dinparasti Saleh, H.; Vezzoli, S.; Caspani, L.; Branny, A.; Kumar, S.; Gerardot, B. D.; Faccio, D. Towards Spontaneous Parametric down Conversion from Monolayer MoS2. *Sci. Rep.* **2018**, *8* (1), 3862.
(15) Hong, H.; Wu, C.; Zhao, Z.; Zuo, Y.; Wang, J.; Liu, C.; Zhang, J.; Wang, F.; Feng, J.; Shen, H.; Yin, J.; Wu, Y.; Zhao, Y.; Liu, K.; Gao, P.; Meng, S.; Wu, S.; Sun, Z.; Liu, K.; Xiong, J. Giant Enhancement of Optical Nonlinearity in Two-Dimensional Materials by Multiphoton-Excitation Resonance Energy Transfer from Quantum Dots. *Nat. Photonics* **2021**, *15* (7), 510−515.
(16) Janisch, C.; Wang, Y.; Ma, D.; Mehta, N.; Elías, A. L.; Perea-López, N.; Terrones, M.; Crespi, V.; Liu, Z. Extraordinary Second Harmonic Generation in Tungsten Disulfide Monolayers. *Sci. Rep.* **2014**, *4* (1), 5530.
(17) Laktaev, I. D.; Saidzhonov, B. M.; Vasiliev, R. B.; Smirnov, A. M.; Butov, O. V. Second Harmonic Generation in Colloidal CdSe/CdS Nanoplatelets. *Results Phys.* **2020**, *19*, 103503.
(18) Murray, W.; Lucking, M.; Kahn, E.; Zhang, T.; Fujisawa, K.; Perea-Lopez, N.; Laura Elias, A.; Terrones, H.; Terrones, M.; Liu, Z. Second Harmonic Generation in Two-Dimensional Transition Metal Dichalcogenides with Growth and Post-Synthesis Defects. *2D Mater.* **2020**, *7* (4), 045020.
(19) Rosa, H. G.; Ho, Y. W.; Verzhbitskiy, I.; Rodrigues, M. J. F. L.; Taniguchi, T.; Watanabe, K.; Eda, G.; Pereira, V. M.; Gomes, J. C. V. Characterization of the Second- and Third-Harmonic Optical Susceptibilities of Atomically Thin Tungsten Diselenide. *Sci. Rep.* **2018**, *8* (1), 10035.
(20) Ullah, K.; Meng, Y.; Shi, Y.; Wang, F. Harmonic Generation in Low-Dimensional Materials. *Adv. Opt. Mater.* **2022**, *10* (7), 2101860.
(21) Wang, Y.; Ghotbi, M.; Das, S.; Dai, Y.; Li, S.; Hu, X.; Gan, X.; Zhao, J.; Sun, Z. Difference Frequency Generation in Monolayer MoS $_2$. *Nanoscale* **2020**, *12* (38), 19638−19643.
(22) Zeng, Z.; Sun, X.; Zhang, D.; Zheng, W.; Fan, X.; He, M.; Xu, T.; Sun, L.; Wang, X.; Pan, A. Controlled Vapor Growth and Nonlinear Optical Applications of Large-Area 3R Phase WS $_2$ and WSe $_2$ Atomic Layers. *Adv. Funct. Mater.* **2019**, *29* (11), 1806874.
(23) Zhou, R.; Krasnok, A.; Hussain, N.; Yang, S.; Ullah, K. Controlling the Harmonic Generation in Transition Metal Dichalcogenides and Their Heterostructures. *Nanophotonics* **2022**, *11* (13), 3007−3034.
(24) Anantharaman, S. B.; Jo, K.; Jariwala, D. Exciton−Photonics: From Fundamental Science to Applications. *ACS Nano* **2021**, *15* (8), 12628−12654.
(25) Kumar, P.; Lynch, J.; Song, B.; Ling, H.; Barrera, F.; Kisslinger, K.; Zhang, H.; Anantharaman, S. B.; Digani, J.; Zhu, H.; Choudhury, T. H.; McAleese, C.; Wang, X.; Conran, B. R.; Whear, O.; Motala, M. J.; Snure, M.; Muratore, C.; Redwing, J. M.; Glavin, N. R.; Stach, E. A.; Davoyan, A. R.; Jariwala, D. Light−Matter Coupling in Large-Area van Der Waals Superlattices. *Nat. Nanotechnol.* **2022**, *17* (2), 182−189.
(26) Fryett, T.; Zhan, A.; Majumdar, A. Cavity Nonlinear Optics with Layered Materials. *Nanophotonics* **2017**, *7* (2), 355−370.
(27) Ge, X.; Minkov, M.; Fan, S.; Li, X.; Zhou, W. Laterally Confined Photonic Crystal Surface Emitting Laser Incorporating Monolayer Tungsten Disulfide. *npj 2D Mater. Appl.* **2019**, *3* (1), 16.
(28) Xia, F.; Wang, H.; Xiao, D.; Dubey, M.; Ramasubramaniam, A. Two-Dimensional Material Nanophotonics. *Nat. Photonics* **2014**, *8* (12), 899−907.
(29) Wang, Q. H.; Kalantar-Zadeh, K.; Kis, A.; Coleman, J. N.; Strano, M. S. Electronics and Optoelectronics of Two-Dimensional Transition Metal Dichalcogenides. *Nat. Nanotechnol.* **2012**, *7* (11), 699−712.
(30) Fryett, T. K.; Seyler, K. L.; Zheng, J.; Liu, C.-H.; Xu, X.; Majumdar, A. Silicon Photonic Crystal Cavity Enhanced Second-Harmonic Generation from Monolayer WSe $_2$. *2D Mater.* **2017**, *4* (1), 015031.
(31) Day, J. K.; Chung, M.-H.; Lee, Y.-H.; Menon, V. M. Microcavity Enhanced Second Harmonic Generation in 2D MoS_2. *Opt. Mater. Express* **2016**, *6* (7), 2360.
(32) Yi, F.; Ren, M.; Reed, J. C.; Zhu, H.; Hou, J.; Naylor, C. H.; Johnson, A. T. C.; Agarwal, R.; Cubukcu, E. Optomechanical Enhancement of Doubly Resonant 2D Optical Nonlinearity. *Nano Lett.* **2016**, *16* (3), 1631−1636.
(33) Liu, C.; Zheng, J.; Chen, Y.; Fryett, T.; Majumdar, A. Van Der Waals Materials Integrated Nanophotonic Devices [Invited]. *Opt. Mater. Express* **2019**, *9* (2), 384.
(34) Wang, Z.; Dong, Z.; Zhu, H.; Jin, L.; Chiu, M.-H.; Li, L.-J.; Xu, Q.-H.; Eda, G.; Maier, S. A.; Wee, A. T. S.; Qiu, C.-W.; Yang, J. K. W. Selectively Plasmon-Enhanced Second-Harmonic Generation from Monolayer Tungsten Diselenide on Flexible Substrates. *ACS Nano* **2018**, *12* (2), 1859−1867.
(35) Shi, J.; Liang, W.; Raja, S. S.; Sang, Y.; Zhang, X.; Chen, C.; Wang, Y.; Yang, X.; Lee, Y.; Ahn, H.; Gwo, S. Plasmonic Enhancement and Manipulation of Optical Nonlinearity in Monolayer Tungsten Disulfide. *Laser Photonics Rev.* **2018**, *12* (10), 1800188.
(36) Löchner, F. J. F.; George, A.; Koshelev, K.; Bucher, T.; Najafidehaghani, E.; Fedotova, A.; Choi, D.-Y.; Pertsch, T.; Staude, I.; Kivshar, Y.; Turchanin, A.; Setzpfandt, F. Hybrid Dielectric Metasurfaces for Enhancing Second-Harmonic Generation in Chemical Vapor Deposition Grown MoS $_2$ Monolayers. *ACS Photonics* **2021**, *8* (1), 218−227.
(37) Li, D.; Wei, C.; Song, J.; Huang, X.; Wang, F.; Liu, K.; Xiong, W.; Hong, X.; Cui, B.; Feng, A.; Jiang, L.; Lu, Y. Anisotropic Enhancement of Second-Harmonic Generation in Monolayer and Bilayer MoS $_2$ by Integrating with TiO $_2$ Nanowires. *Nano Lett.* **2019**, *19* (6), 4195−4204.
(38) Bernhardt, N.; Koshelev, K.; White, S. J. U.; Meng, K. W. C.; Fröch, J. E.; Kim, S.; Tran, T. T.; Choi, D.-Y.; Kivshar, Y.; Solntsev, A. S. Quasi-BIC Resonant Enhancement of Second-Harmonic Generation in WS $_2$ Monolayers. *Nano Lett.* **2020**, *20* (7), 5309−5314.
(39) Akselrod, G. M.; Ming, T.; Argyropoulos, C.; Hoang, T. B.; Lin, Y.; Ling, X.; Smith, D. R.; Kong, J.; Mikkelsen, M. H. Leveraging Nanocavity Harmonics for Control of Optical Processes in 2D Semiconductors. *Nano Lett.* **2015**, *15* (5), 3578−3584.
(40) Shradha, S.; Abtahi, F.; Gan, Z.; Knopf, H.; Fedotova, A.; Löchner, F. J. F.; George, A.; Pertsch, T.; Turchanin, A.; Eilenberger, F. Towards Double Resonant Cavity Enhanced Second Harmonic Generation in Monolayer MoS $_2$. *Adv. Opt. Mater.* **2023**, 2300907.

https://doi.org/10.1021/acsphotonics.4c01029
ACS Photonics 2024, 11, 4635−4641

(41) Khurgin, J. B. Nonlinear Optics from the Viewpoint of Interaction Time. *Nat. Photonics* **2023**, *17* (7), 545−551.
(42) Quan, Q.; Loncar, M. Deterministic Design of Wavelength Scale, Ultra-High Q Photonic Crystal Nanobeam Cavities. *Opt. Express* **2011**, *19* (19), 18529.
(43) Zhou, J.; Zheng, J.; Fang, Z.; Xu, P.; Majumdar, A. Ultra-Low Mode Volume on-Substrate Silicon Nanobeam Cavity. *Opt. Express* **2019**, *27* (21), 30692.
(44) Rosser, D.; Fryett, T.; Ryou, A.; Saxena, A.; Majumdar, A. Exciton−Phonon Interactions in Nanocavity-Integrated Monolayer Transition Metal Dichalcogenides. *npj 2D Mater. Appl.* **2020**, *4* (1), 20.

https://doi.org/10.1021/acsphotonics.4c01029
ACS Photonics 2024, 11, 4635−4641